Chinese Chemical Letters 36 (2025) 110082

Contents lists available at ScienceDirect

Chinese Chemical Letters

journal homepage: www.elsevier.com/locate/cclet

Rationally designed an innovative proximity labeling near-infrared fluorogenic probe for imaging of peroxynitrite in acute lung injury

Dandan Tang[a,b,1], Ningge Xu[a,b,1], Yuyang Fu[b], Wei Peng[b], Jinsheng Wu[a], Heng Liu[a,b,*], Fabiao Yu[a,b,*]

[a] Key Laboratory of Emergency and Trauma of Ministry of Education, Department of Radiotherapy, The First Affiliated Hospital of Hainan Medical University, Hainan Medical University, Haikou 571199, China
[b] Key Laboratory of Hainan Trauma and Disaster Rescue, Key Laboratory of Haikou Trauma, Engineering Research Center for Hainan Bio-Smart Materials and Bio-Medical Devices, College of Emergency and Trauma, Hainan Medical University, Haikou 571199, China

ARTICLE INFO

Article history:
Received 8 April 2024
Revised 30 May 2024
Accepted 2 June 2024
Available online 3 June 2024

Keywords:
Near-infrared
Peroxynitrite
Proximity labeling
In situ bioimaging
Acute lung injury

ABSTRACT

Acute lung injury (ALI) is a serious clinical condition with a high mortality rate. Oxidative stress and inflammatory responses play pivotal roles in the pathogenesis of ALI. $ONOO^-$ is a key mediator that exacerbates oxidative damage and microvascular permeability in ALI. Accurate detection of $ONOO^-$ would facilitate early diagnosis and intervention in ALI. Near-infrared fluorescence (NIRF) probes offer new solutions due to their sensitivity, depth of tissue penetration, and imaging capabilities. However, the developed $ONOO^-$ fluorescent probes face problems such as interference from other reactive oxygen species and easy intracellular diffusion. To address these issues, we introduced an innovative self-immobilizing NIRF probe, DCI2F-OTf, which was capable of monitoring $ONOO^-$ *in vitro* and *in vivo*. Importantly, leveraging the high reactivity of the methylene quinone (QM) intermediate, DCI2F-OTf was able to covalently label proteins in the presence of $ONOO^-$, enabling *in situ* imaging. In mice models of ALI, DCI2F-OTf enabled real-time imaging of $ONOO^-$ levels and found that $ONOO^-$ was tightly correlated with the progression of ALI. Our findings demonstrated that DCI2F-OTf was a promising chemical tool for the detection of $ONOO^-$, which could help to gain insight into the pathogenesis of ALI and monitor treatment efficacy.

Acute lung injury (ALI) refers to the injury of alveolar epithelial cells and capillary endothelial cells caused by various non-cardiogenic factors, with a high mortality rate [1]. Clinically, ALI can rapidly progress to acute respiratory distress syndrome, a more severe form of lung injury. Oxidative stress and exaggerated inflammatory responses are recognized as pivotal contributors to the pathogenesis and exacerbation of ALI [2,3]. In biological systems, the rapid diffusion of nitric oxide (NO) and superoxide anions produces endogenous $ONOO^-$, a potent reactive species generated at a rate hundreds of times faster than the rate of NO binding to heme protein. $ONOO^-$ readily engages in reactions with proteins, lipids, or nucleic acids to promote oxidation or nitration of biomolecules that can lead to cellular damage. For instance, $ONOO^-$ can alter the structure of proteins through the formation of nitrifying proteins, thus affecting their physiological function [4–8]. $ONOO^-$ acts as a signaling molecule to participate in cell signal transduction and various physiological processes, including gene expression regulation and apoptosis [9]. On one hand, elevated levels of $ONOO^-$ disrupt the lung's antioxidant defense system, exacerbating oxidative stress and cellular damage; on the other hand, increased $ONOO^-$ levels significantly enhance the permeability of the lung microvascular wall, which ultimately impairs lung function [10–14]. Thus, the development of innovative tools for the detection of $ONOO^-$ to accurately diagnose ALI will help to track disease progression in time for early intervention and improve patient survival.

Fluorescent probes have emerged as a powerful tool for visualizing diverse physiological and pathological processes due to their high sensitivity, non-invasiveness, and real-time imaging capabilities. Particularly, near-infrared fluorescent (NIRF) probes offer superior optical penetration, less photodamage, and lower background fluorescence. In recent years, a variety of $ONOO^-$-fluorescent probes have been constructed leveraging diverse reaction moieties, including unsaturated double bonds, boronic esters, boronic acids, hydrazines, and so on [15–25]. However, available $ONOO^-$-fluorescent probes encounter two primary challenges: (1)

* Corresponding authors.
E-mail addresses: liuheng@hainmc.edu.cn (H. Liu), yufabiao@hainmc.edu.cn (F. Yu).
[1] These authors contributed equally to this work.

https://doi.org/10.1016/j.cclet.2024.110082
1001-8417/

susceptible to potential interference from high concentrations of reactive oxygen species (*e.g.*, hypochlorite, hydrogen peroxide); (2) prone to diffuse from the reaction site, thereby decreasing imaging accuracy and signal-to-noise ratio. Hence, it is of great importance to design $ONOO^-$-activated, proximity protein-captured, self-immobilizing NIRF probes at the cellular or *in vivo* level.

Methylene quinone (QM) is an important class of electrophilic intermediates with high reactivity in chemical reactions. In biological applications, the QM released from the reaction of a chemical probe with physiologically reactive species is easily trapped by nucleophilic groups in nearby protein molecules [26–29]. This strategy has been widely used in the design and synthesis of *in situ* labeling probes for hydrogen peroxide [30], neuraminidases [31], β-galactosidase [32], nitroreductase [33], γ-glutamyl transpeptidase [34], and alkaline phosphatase [35]. Inspired by these pioneering efforts, we herein disclosed a novel activatable self-immobilizing NIRF probe DCI2F-OTf for the detection of $ONOO^-$ *in vitro* and *in vivo*. In this design, dicyanoisophorone derivatives (DCI) were adopted as a NIRF signaling unit due to their excellent stability, large Stoke shift, and ease of synthesis, while trifluoromethane sulfonate was employed as the reactive moiety for $ONOO^-$ owing to its ultra-high selectivity. The molecular design of DCI2F-OTf facilitated its implementation for precise imaging of $ONOO^-$ in cells and mice model of ALI. NIRF imaging allowed DCI2F-OTf to successfully visualize changes in $ONOO^-$ levels in both cells and mice model of ALI. Furthermore, DCI2F-OTf could serve as an indicator to tracer the protective effect of sulforaphane (SFN) on lipopolysaccharide (LPS)-induced ALI in mice. These findings suggested that DCI2F-OTf could be used as a promising tool to obtain information about oxidative stress-related diseases and to track the effects of drug therapy.

Two DCI-type fluorescence probes DCI2F-OTf and DCI-OTf were designed and synthesized. The chemical structures of all compounds were comprehensively characterized by nuclear magnetic resonance (NMR) and high-resolution mass spectroscopy (HRMS) (Figs. S1–S6 in Supporting information). Of note, the fluorescence response of DCI-OTf to $ONOO^-$ was minimal and spectrally blue-shifted to 525 nm compared to DCI2F-OTf, whereas DCI2F-OTf exhibited excellent selectivity, sensitivity, and NIRF emission characteristics (Fig. S8 in Supporting information). We hypothesized that this disparity could be attributed to the electron-withdrawing difluoromethyl (-CHF2) in the *ortho* position of the hydroxyl group, which was able to effectively reduce the pK_a value of DCI2F-OTf, enhance its reactivity toward $ONOO^-$, and lower the detection limit of $ONOO^-$. It was widely known that $ONOO^-$ itself was oxidizing and nucleophilic. In this design, the sulfur-centered atom of the positively charged trifluoromethanesulfonyl group was initially attacked by the nucleophile $ONOO^-$, and then underwent a nucleophilic addition-elimination reaction, which cleaved the sulfur-oxygen bond to delocalize the trifluoromethanesulfonyl group, forming the key intermediate DCI2F. Subsequently, the DCI2F underwent intramolecular rearrangement to generate the QM, which was captured by nucleophilic groups (*e.g.*, hydroxyl, amine, and sulfhydryl groups) around the active site of the protein within cells, facilitating *in situ* imaging (Scheme 1). To elucidate the reaction mechanism of DCI2F-OTf with $ONOO^-$, the mixture of DCI2F-OTf reacting with $ONOO^-$ was analyzed by HRMS. The results revealed a mass peak at $m/z = 361.1372$, which was attributed to DCI-H_2O and different from the mass peak of DCI2F-OTf at $m/z = 472.0889$. The plausible reaction mechanism involved the reaction of DCI2F-OTf with $ONOO^-$ to release QM, followed by nucleophilic attack by H_2O in the mixed system to form the product DCI-H_2O, consistent with the mechanism of protein capture of QM (Fig. S7 in Supporting information).

The change of fluorescence emission spectra of DCI2F-OTf toward $ONOO^-$ was first measured. DCI2F-OTf hardly fluoresced

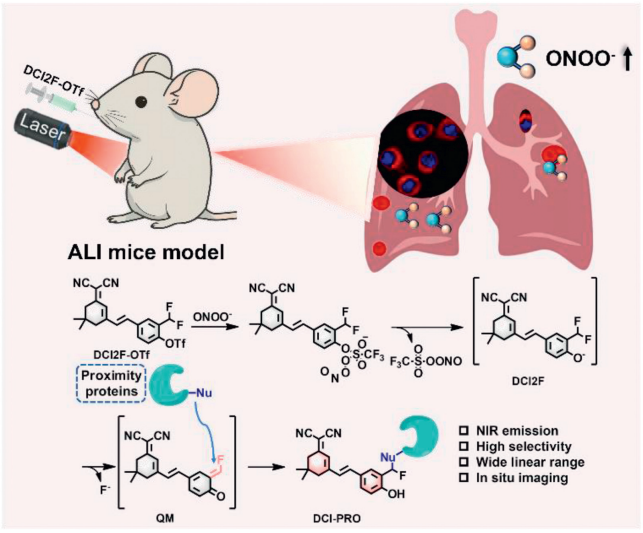

Scheme 1. Schematic illustration of dual sensing and labeling NIRF probe DCI2F-OTf for $ONOO^-$.

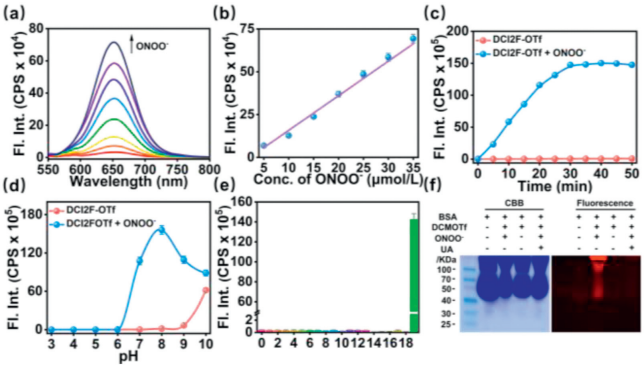

Fig. 1. Fluorescence response of DCI2F-OTf (10 μmol/L) to $ONOO^-$ excited at 490 nm. (a) Visualization of the fluorescence changes of DCI2F-OTf during titration with increasing $ONOO^-$ (0–35 μmol/L) concentrations. (b) Linearity of the fluorescence intensity value of DCI2F-OTf at 652 nm with varied concentrations of $ONOO^-$ (5–35 μmol/L). (c) Time-dependent fluorescence response of DCI2F-OTf before and after the addition of $ONOO^-$ (70 μmol/L) at 37 °C recorded every 5 min. (d) The fluorescence intensities at 652 nm of DCI2F-OTf in the absence or presence of $ONOO^-$ (70 μmol/L) over pH range from 3.0 to 7.0. (e) Values of fluorescence intensities of DCI2F-OTf treated with different competitive biological agents: 1. blank, 2. Na^+ (500 μmol/L), 3. K^+ (500 μmol/L), 4. Ser (200 μmol/L), 5. Leu (200 μmol/L), 6. Arg (200 μmol/L), 7. $S_2O_3^{2-}$ (100 μmol/L), 8. HSO_3^- (100 μmol/L), 9. H_2S (100 μmol/L), 10. Cys (100 μmol/L), 11. GSH (1 mmol/L), 12. NO_2^- (100 μmol/L), 13. NO_3^- (100 μmol/L), 14. NO (100 μmol/L), 15. $^{\cdot}OH$ (100 μmol/L), 16. O_2^1 (100 μmol/L), 17. H_2O_2 (100 μmol/L), 18. $O_2^{\cdot-}$ (100 μmol/L), 19. HOCl (100 μmol/L), 20. $ONOO^-$ (70 μmol/L). (f) SDS-PAGE analysis of BSA (5 mg/mL) after incubation with DCI2F-OTf + $ONOO^-$, DCI2F-OTf, DCI2F-OTf + $ONOO^-$ + UA in PBS at 37 °C for 30 min. Left: Coomassie brilliant blue staining; right: fluorescence imaging.

due to the hydroxyl group of the fluorophore DCI masked by the -SO_2CF_3 group. Upon the incremental addition of $ONOO^-$ (0–35 μmol/L), the emission signal of DCI2F-OTf at 652 nm was gradually intensified to nearly 22-fold (Fig. 1a). Interestingly, the addition of $ONOO^-$ (35–70 μmol/L) gave a sharp enhancement of the emission signal of DCI2F-OTf (Figs. S9 and S10 in Supporting information). A gradual change in the color of the solution of DCI2F-OTf from colorless to pink was observed with the naked eye as the $ONOO^-$ concentration. At the same time, the red fluorescence of the solution deepened under a 365 nm ultraviolet lamp (Fig. S11 in Supporting information). The fluorescence intensity at 652 nm linearly increased with $ONOO^-$ concentration ranging from 5 μmol/L to 35 μmol/L (Fig. 1b). The linear regression equation was $F_{652\ nm}/10{,}000 = 2.019\ [ONOO^-] - 4.405$ with a correlation coeffi-

cient of 0.9906, yielding a detection limit of 96 nmol/L for $ONOO^-$ based on 3σ/k. This indicated that DCI2F-OTf featured a high response sensitivity to $ONOO^-$ and great potential for quantitative analysis. Following the addition of $ONOO^-$ to a solution of DCI2F-OTf induced a rapid increase in emission signal and then arrived at a plateau within 30 min (Fig. 1c). The final response time chosen for the spectroscopic test was 30 min. The emission signal of DCI2F-OTf at 652 nm shifted insignificantly across a pH range of 3.0–9.0 (Fig. 1d). At pH 10.0, a noticeable enhancement in the emission signal of DCI2F-OTf was observed, owing to the strong alkaline environment prompting the hydrolysis of the $-SO_2CF_3$ group and subsequent release of the fluorophore. The response of DCI2F-OTf to $ONOO^-$ was inhibited in the acidic pH range of 3.0–6.0, while the emission signal of DCI2F-OTf was increased and then declined over a pH range of 6.0–10.0. Notably, the maximum response value was reached near pH 7.4, which meant that DCI2F-OTf could sense $ONOO^-$ under physiological conditions. To assess the specificity of DCI2F-OTf reaction with $ONOO^-$, a series of competitive biological agents, such as Na^+, K^+, Ser, Leu, Arg, $S_2O_3^{2-}$, HSO_3^-, H_2S, Cys, GSH, NO_2^-, NO_3^-, NO, $^{\bullet}OH$, $O_2{}^1$, H_2O_2, $O_2^{\bullet-}$, HOCl, were opted to determine their effect on fluorescence response. It was clear from Fig. 1e that the optical response of the interferents to DCI2F-OTf was negligible, and only the addition of $ONOO^-$ led to a significant emission signal change of DCI2F-OTf, thus indicating that DCI2F-OTf presented a well-selective response to $ONOO^-$. Taken together, DCI2F-OTf held promise as a potential chemical tool for the detection of $ONOO^-$ in living systems. Subsequently, employing bovine serum albumin (BSA) as a model protein substrate and with the aid of sodium dodecyl sulfate-polyacrylamide gel electrophoresis (SDS-PAGE) analysis of the reaction product, we verified the ability of DCI2F-OTf to covalently label proximity proteins in the presence of $ONOO^-$ (Fig. 1f). A distinct fluorescent protein band was observed *via* in-gel fluorescence imaging only in the coexistence of BSA, DCI2F-OTf, and $ONOO^-$, whereas the fluorescence signal was notably diminished in the presence of uric acid (UA, a well-known antioxidant capable of removing $ONOO^-$) [36]. These findings proved that DCI2F-OTf was an $ONOO^-$-responsive and $ONOO^-$-dependent protein labeling NIRF probe.

Having confirmed the ability of DCI2F-OTf to successfully covalently label proteins in the presence of $ONOO^-$, we proceeded to perform cell-based imaging studies. Before cell imaging, a cell counting kit-8 (CCK-8) assay was applied to assess the cytotoxicity of DCI2F-OTf, and it was found that DCI2F-OTf did not significantly reduce the survival of the cells up to a concentration of 30 μmol/L (Fig. S12 in Supporting information). RAW264.7 and A549 cells were chosen to fluorescence image $ONOO^-$ at the cellular level. The ability of DCI2F-OTf and DCI-OTf to image $ONOO^-$ was first compared (Fig. 2a). The cells were pretreated with 3-morpholinosydnonimine (SIN-1) or lipopolysaccharide/interferon-γ/phorbol 12-myristate 13-acetate (LPS/IFN-γ/PMA), and then stained with DCI2F-OTf and DCI-OTf, respectively. In comparison with the control group, it was found that upon pretreatment with SIN-1 or LPS/IFN-γ/PMA, the fluorescence signal of DCI-OTf was negligible, while DCI2F-OTf displayed marked fluorescence enhancement, indicative of the excellent imaging capability of DCI2F-OTf for $ONOO^-$. Subsequently, the capability of DCI2F-OTf to covalently label proximity proteins in A549 cells was investigated (Fig. 2b). DCM-KA, which has no difluoromethyl functional group in its molecular structure, was selected as a control compound (Fig. S13 in Supporting information) [37]. A549 cells were sequentially incubated with SIN-1 and DCM-KA, and the fluorescence signal decayed rapidly after washout with DMEM. DCI2F-OTf retained a relatively robust fluorescence emission even after washout with DMEM, which was attributed to the covalent anchoring of the QM

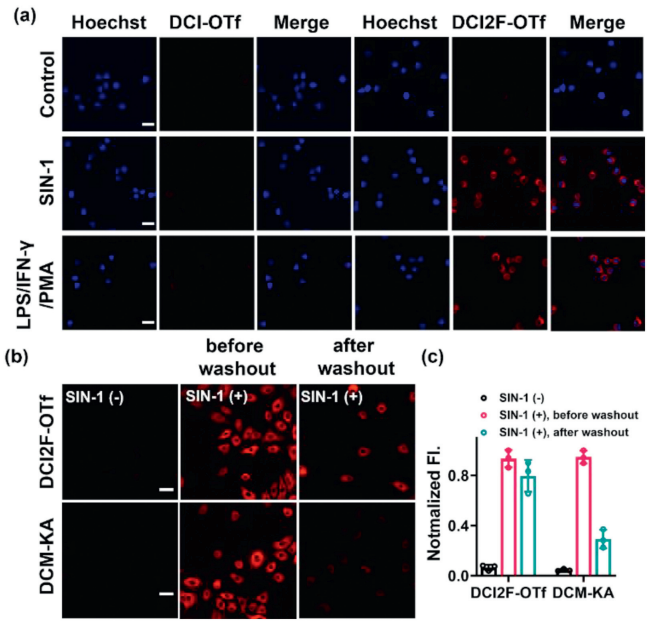

Fig. 2. (a) RAW264.7 cells were pretreated with SIN-1 (200 μmol/L, 30 min) or stimulated with LPS (1.0 μg/mL), IFN-γ (100 ng/mL) for 12 h, PMA (10 nmol/L) for 30 min, and then incubated with DCI-OTf (10 μmol/L, 30 min) or DCI2F-OTf (10 μmol/L, 30 min), respectively. The red channel was collected in the range of 600–700 nm for DCI2F-OTf, 500–600 nm for DCI-OTf (λ_{ex} = 488 nm), and the Hoechst channel was collected in the range of 430–480 nm (λ_{ex} = 405 nm). (b) A549 cells were pretreated with SIN-1 (200 μmol/L, 30 min), followed by incubation with DCI2F-OTf (10 μmol/L, 30 min) or DCM-KA (10 μmol/L, 30 min), before or after washout with fresh DMEM (3 times, each for 6 min). Scale bar: 50 μm. (c) Normalized fluorescence intensity plots of DCI2F-OTf and DCM-KA labeled cells in (b). Data are presented as mean ± standard deviation (SD) (n = 3).

intermediate generated by the reaction of DCI2F-OTf with $ONOO^-$ to proximity proteins (Fig. 2c).

Following this, imaging of exogenous $ONOO^-$ was explored with the aid of DCI2F-OTf. As illustrated in Figs. 3a and b, the red fluorescence signal originating from the cells progressively enhanced as exogenous $ONOO^-$ donor SIN-1 concentration increased from 50 μmol/L to 200 μmol/L, while the cells co-incubated with the commercial $ONOO^-$ scavenger ebselen showed varying degrees of diminished red fluorescence signal [38]. Using DCI2F-OTf, similar imaging results were obtained in A549 cells (Fig. S14 in Supporting information). Immunoblotting analysis results further confirmed the protein expression level of interleukin-6 (IL-6) and inducible nitric oxide synthase (iNOS) were up-regulated, which was significantly higher than that of control and ebselen-treated groups (Figs. 3c and d). This suggested that SIN-1 could induce cellular oxidative stress and inflammatory response, whereas ebselen effectively scavenged reactive oxygen species (ROS) and reduced the expression of inflammatory cytokines, exerting anti-inflammatory and antioxidant effects, consistent with the results of confocal laser scanning microscopy (CLSM) images. Real-time images of DCI2F-OTf incubated with the cells in the presence of $ONOO^-$ for 30 min were recorded (Fig. 3e). The red fluorescence signal gradually intensified as the incubation time extended from 6 min to 30 min. The results of flow cytometry also revealed a gradual increase in the fluorescence of DCI2F-OTf labeled cells over time (Fig. 3f).

LPS was a potent immunostimulant capable of eliciting inflammatory response. During the inflammatory response, LPS stimulation could activate a variety of cell types, most typically RAW264.7 cells, resulting in an elevation of $ONOO^-$ levels [39,40]. DCI2F-OTf was exploited to monitor subtle concentration changes of $ONOO^-$ in LPS-stimulated cells. As depicted in Fig. 4a, almost no

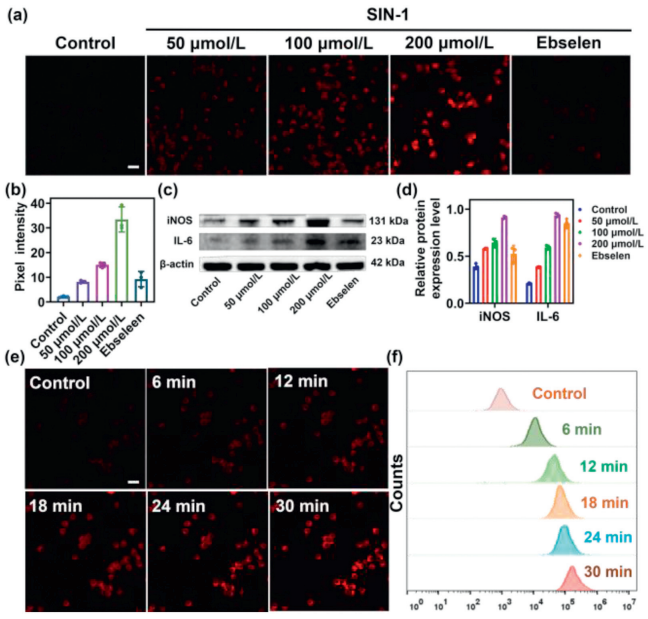

Fig. 3. (a) RAW264.7 cells pretreated with different concentrations of SIN-1 (0, 50, 100, 200 μmol/L), SIN-1 (200 μmol/L) plus ebselen (200 μmol/L) for 30 min were incubated with DCI2F-OTf (10 μmol/L) for 30 min. (b) The pixel intensity of DCI2F-OTf labeled cells in (a). (c) The protein levels of iNOS and IL-6 were detected by Western blot analysis. (d) The relative protein expression level of iNOS and IL-6 in (c). (e) RAW264.7 cells were pretreated with SIN-1 (200 μmol/L, 30 min), and then incubated with DCI2F-OTf (10 μmol/L) for 0–30 min. (f) Flow cytometry analysis of DCI2F-OTf (10 μmol/L) labeled SIN-1 (200 μmol/L, 30 min) pretreated cells. Data are presented as mean ± SD ($n = 3$). Scale bar: 50 μm.

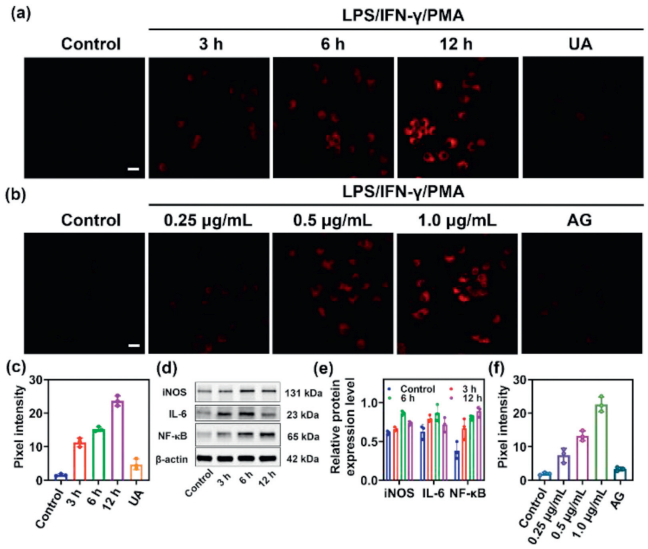

Fig. 4. (a) RAW264.7 cells were pretreated with the stimulus LPS (1.0 μg/mL)/IFN-γ (100 ng/mL) for different periods (0, 3, 6, 12 h), PMA (10 nmol/L) for 30 min or LPS (1.0 μg/mL)/IFN-γ (100 ng/mL) plus UA (200 μmol/L) for 12 h, PMA (10 nmol/L) for 30 min, and then incubated with DCI2F-OTf (10 μmol/L) for 30 min. (b) RAW264.7 cells were pretreated with LPS (0, 0.25, 0.5, 1.0 μg/mL)/IFN-γ (100 ng/mL), PMA (10 nmol/L), or LPS (1.0 μg/mL)/IFN-γ (100 ng/mL) plus AG (1 mmol/L) for 12 h, PMA (10 nmol/L) for 30 min, and then incubated with DCI2F-OTf (10 μmol/L) for 30 min. (c) The pixel intensity of DCI2F-OTf labeled cells in (a). (d) The protein levels of iNOS, IL-6, and NF-κB were detected by Western blot analysis. (e) The relative protein expression level of iNOS, IL-6, and NF-κB in (c). (f) The pixel intensity of DCI2F-OTf labeled cells in (b). Data are presented as mean ± SD ($n = 3$). Scale bar: 50 μm.

detectable red fluorescence signal was observed in the control group. The cells pretreated with LPS for different durations (3, 6, 12 h) and then treated with IFN-γ/PMA presented a progressive enhancement of the red fluorescence signal. Conversely, the cells treated with LPS/IFN-γ/PMA and UA gave relatively weak red fluorescence signals (Fig. 4c). The immunoblotting analysis provided further insights into the possible mechanism of underlying LPS-mediated upregulation of $ONOO^-$ levels. As depicted in Figs. 4d and e the expression level of protein, IL-6, and iNOS reached the highest at 6 h of LPS treatment, while nuclear factor kappa-B (NF-κB) expression reached its maximum at 12 h of LPS treatment. LPS/IFN-γ/PMA successfully induced the transformation of RAW 264.7 cells into M1-type proinflammatory macrophages, which generated excessive $ONOO^-$ through promoting the expression of inflammatory cytokines. Moreover, the continuous production of IL-6 and iNOS further activated the NF-κB signaling pathway and increased the production of $ONOO^-$. Additionally, LPS dose-dependent changes in cellular fluorescence signal were investigated (Fig. 4b). The red fluorescence signal of the cells was sharply enhanced with increasing LPS concentration from 0.25 μg/mL to 1.0 μg/mL. The addition of aminoguanidine (AG) significantly attenuated the fluorescence signal (Fig. 4f) [41]. Collectively, DCI2F-OTf offered favorable cell permeability and was suitable for the detection of $ONOO^-$ in cells.

LPS stimulation was considered an effective strategy for establishing clinically relevant ALI animal models through inflammation [42]. Motivated by the excellent *in vitro* detection performance, we further assessed the capability of DCI2F-OTf for diagnosing and therapeutic monitoring ALI *in vivo*. All surgical procedures and experimental protocols were approved by the Animal Care and Use Committee of Hainan Medical University (No. HYLL-2021–184). Prior to *in vivo* imaging, the biocompatibility of DCI2F-OTf was first evaluated. Following intravenous injection of DCI2F-OTf, the major organs of the mice were analyzed histologically using hematoxylin and eosin (H&E) staining. It could be seen from Fig. S15 (Supporting information) that there were no obvious abnormalities between the injected DCI2F-OTf group and the normal group, indicative of satisfactory biosafety and suitable for *in vivo* bioimaging. Next, 8-week-old BALB/c mice of ALI were established by intratracheal LPS instillation. The mice were divided into five experimental groups: control group (saline-treated), LPS6 group (LPS-stimulated for 6 h), LPS12 group (LPS-stimulated for 12 h), LPS24 group (LPS-stimulated for 24 h), and LPS + SFN group (SFN-treated). As observed in Fig. 5a, the NIR fluorescence signal in the lungs of mice was found to be rapidly intensified within 30 min and then gradually weakened by intratracheal drip injection of DCI2F-OTf. This decline in fluorescence signal with the extension of time might be attributed to the metabolism of DCI2F-OTf. Compared to the control group, the LPS-stimulated group (LPS6, LPS12, LPS24 group) exhibited different degrees of fluorescence signal enhancement at different time points, with the strongest signal observed at 6 h. The fluorescence signals of mice in the LPS + SFN group were significantly lower than those in the LPS-stimulated group (Fig. 5c). Furthermore, by comparatively analyzing the fluorescence signal intensities of various major organs in dissected mice, it was also evidenced that the fluorescence signals in the lungs of the LPS-stimulated group were much higher than those of the other organs (heart, kidney, liver, spleen), consistent with the results of the *in vivo* imaging experiments (Figs. 5b and d).

For histological analysis of lung tissue sections from different groups of mice demonstrated in Fig. 5e, the LPS-stimulated group exhibited typical ALI alterations, including inflammatory cell infiltration and interstitial lung edema, whereas the LPS + SFN group attenuated the pathological changes. As we know, the expression of inflammatory cytokines was increased at the onset of ALI, and elevated levels of inflammatory cytokines exacerbated the inflam-

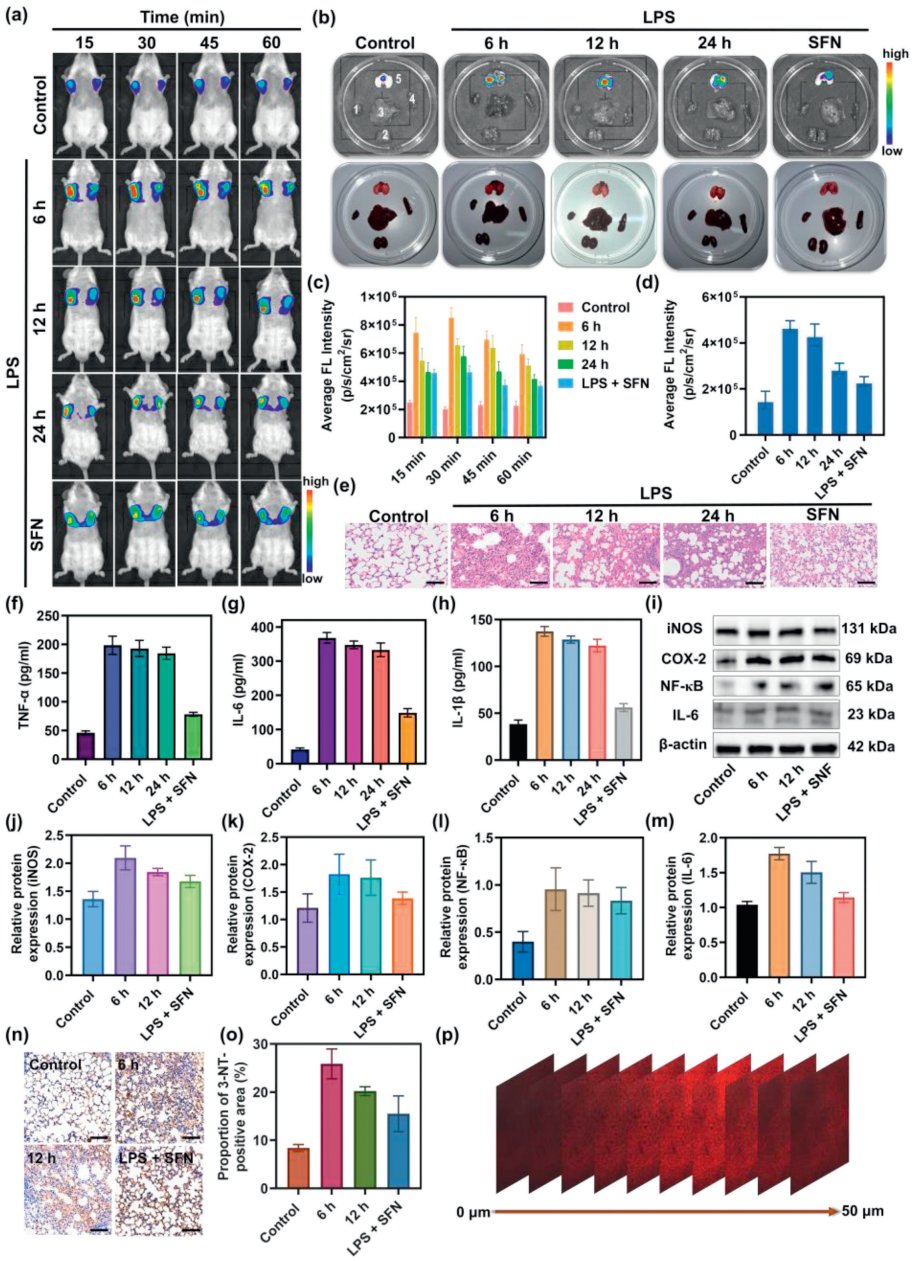

Fig. 5. (a) NIRF images of control and LPS-stimulated mice after intratracheal drip injection of DCI2F-OTf (200 μmol/L, 45 μL). (b) NIRF imaging and photographs of dissected major organs (1: heart, 2: kidney, 3: liver, 4: spleen, 5: lung) from mice in panel (a). (c) The histogram presents the average radiant efficiency of mice in panel (a). (d) The histogram presents the average radiant efficiency of the lung in panel (b). (e) H&E staining histological images for lung tissue in control and LPS-stimulated mice. Scale bar: 50 μm. (f–h) Serum levels of inflammatory factors TNF-α, IL-6, and IL-1β in control and LPS-stimulated mice. (i) The protein levels of iNOS, COX-2, NF-κB, and IL-6 were detected by Western blot analysis. (j–m) The relative protein expression level of iNOS, COX-2, NF-κB, and IL-6 in (i). (n, o) Sections of lung tissue were immunostained with an antibody that detected 3-NT. Scale bar: 50 μm. (p) NIRF images of mice fresh lung tissue sections from ALI mice in the LPS6 group. The confocal Z-axis scan images at 0, 5, 10, 15, 20, 25, 30, 35, 40, and 50 μm penetration depths. $\lambda_{ex} = 488$ nm; red channel: $\lambda_{em} = 600–700$ nm. Data are presented as mean ± SD ($n = 3$).

matory response and further promoted the development of ALI. Subsequently, an enzyme-linked immunosorbent assay (ELISA) assay was employed to measure the levels of key inflammatory cytokines in the serum of mice. As seen in Figs. 5f–h, tumor necrosis factor-α (TNF-α), IL-6, and IL-1β levels were significantly upregulated in the LPS-stimulated group compared to the control group. Following SFN treatment, TNF-α, IL-6, and IL-1β levels decreased noticeably, suggesting that SFN could downregulate TNF-α, IL-6, and IL-1β expression levels in ALI mice. The activity of iNOS directly impacted the synthesis and release of NO, which was closely related to the production of NO and $ONOO^-$. ALI might trigger lung injury by activating the NF-κB signaling pathway, and the activation of NF-κB increased the expression of cyclooxygenase-2 (COX-2) and IL-6. The results of Western blot analysis in Figs. 5i–m revealed that the protein expression levels of iNOS, COX-2, NF-κB, and IL-6 were upregulated in the LPS-stimulated group; the protein expression levels of iNOS, COX-2, NF-κB, and IL-6 were decreased in the LPS + SFN group compared with the LPS-stimulated group, which meant that SFN probably inhibited the inflammatory response by modulating the NF-κB signaling pathway. 3-Nitrotyrosine (3-NT) was a product of nitrosative stress injury and served as an indicator to analyze the degree of $ONOO^-$ production. Immunohistochemistry results found that the expression level of 3-NT in the lung tissues of mice in the LPS-

stimulated group increased over time, whereas the expression in the LPS + SFN group was relatively low (Figs. 5n and o). This indicated that SFN would effectively reduce $ONOO^-$ production to counteract nitrosative stress injury. Fluorescence imaging of mice fresh lung tissue sections from ALI mice in the LPS6 group further demonstrated that DCI2F-OTf could image tissues with a penetration depth of nearly 50 μm (Fig. 5p). Taken together, these data demonstrated that DCI2F-OTf was a reliable chemical tool for real-time monitoring of $ONOO^-$ and tracking the progression of ALI.

In conclusion, we have designed a novel NIRF probe, DCI2F-OTf, for fluorescence imaging $ONOO^-$ in live cells and mice model of ALI. Under physiological conditions, DCI2F-OTf was highly sensitive and selective for $ONOO^-$ and yielded a linear response to ONOO over a wide concentration range from 0 to 70 μmol/L. The QM covalently labeled neighboring proteins released from the reaction of DCI2F-OTf with $ONOO^-$ could solve the problem of intracellular diffusion of the probe, enabling precise imaging of intracellular $ONOO^-$. This strategy was superior to the vast majority of $ONOO^-$ probes that have been developed so far. The excellent sensing performance and NIRF emission characteristics enabled DCI2F-OTf to image $ONOO^-$ levels in mice and tissues with ALI. *In vivo* imaging results indicated that SFN significantly down-regulated the oxidative stress level, attenuating the severity of LPS-induced ALI, and could exert a protective role against ALI. Therefore, DCI2F-OTf was a valuable tool for studying the physiological function of $ONOO^-$ and was expected to facilitate the understanding of oxidative stress diseases such as ALI and the rapid screening of corresponding therapeutic drugs.

Declaration of competing interest

The authors declare that they have no known competing financial interests or personal relationships that could have appeared to influence the work reported in this paper.

CRediT authorship contribution statement

Dandan Tang: Writing – original draft, Investigation, Data curation, Conceptualization. **Ningge Xu:** Writing – original draft, Investigation, Data curation. **Yuyang Fu:** Validation, Data curation. **Wei Peng:** Data curation. **Jinsheng Wu:** Writing – review & editing, Resources. **Heng Liu:** Writing – review & editing, Supervision, Resources, Project administration, Funding acquisition, Conceptualization. **Fabiao Yu:** Writing – review & editing, Supervision, Funding acquisition, Conceptualization.

Acknowledgments

This work was supported by the National Natural Science Foundation of China (Nos. 22264013, 21961010), Hainan Province Science and Technology Special Fund (Nos. ZDYF2021SHFZ219, ZDYF2022SHFZ037), Special Funds of S&T Cooperation and Exchange Projects of Shanxi Province (No. 202204041101040), Natural Science Research Talent Project of Hainan Medical University (No. JBGS202101), Postgraduate Innovative Research Project of Hainan (No. Qhys2021–384), Hainan Province Clinical Medical Center (2021), and Project for Functional Materials and Molecular Imaging Science Innovation Group of Hainan Medical University. Thanks to the support and assistance in terms of instruments and facilities provided by Public Research Center of Hainan Medical University.

Supplementary materials

Supplementary material associated with this article can be found, in the online version, at doi:10.1016/j.cclet.2024.110082.

References

[1] N.T. Mowery, W.T.H. Terzian, A.C. Nelson, Curr. Probl. Surg. 57 (2020) 100777.
[2] L.D. Bos, L.B. Ware, Lancet 400 (2022) 1145–1156.
[3] F.S. Bezerra, M. Lanzetti, R.T. Nesi, et al., Antioxidants 12 (2023) 548.
[4] N. Hogg, J. Zielonka, B. Kalyanaraman, Chapter 3 - Detection of nitric oxide and peroxynitrite in biological systems: A state-of-the-art review, in: L.J. Ignarro, B.A. Freeman (Eds.), Nitric Oxide: Biology and Pathobiology, Third Edition, Academic Press, 2017, pp. 23–44.
[5] P.G. Wang, M. Xian, X. Tang, et al., Chem. Rev. 102 (2002) 1091–1134.
[6] P. Pacher, J.S. Beckman, L. Liaudet, Physiol. Rev. 87 (2007) 315–424.
[7] G. Ferrer-Sueta, N. Campolo, M. Trujillo, et al., Chem. Rev. 118 (2018) 1338–1408.
[8] R. Radi, J.S. Beckman, K.M. Bush, et al., Arch. Biochem. Biophys. 288 (1991) 481–487.
[9] L. Fialkow, Y. Wang, G.P. Downey, Free. Radical. Biol. Med. 42 (2007) 153–164.
[10] A. van der Vliet, Chapter 25 - antioxidant defenses in the lung, in: R.A. Parent (Ed.), Comparative Biology of the Normal Lung, 2nd Edition, Academic Press, San Diego, 2015, pp. 489–507.
[11] H.S. Park, S.R. Kim, Y.C. Lee, Respirology 14 (2009) 27–38.
[12] S. Zhu, M. Manuel, S. Tanaka, et al., Environ. Health. Perspect. 106 (1998) 1157–1163.
[13] A. van der Vliet, J.P. Eiserich, C.E. Cross, Respir. Res. 1 (2000) 1.
[14] J. Joffre, J. Hellman, Antioxid. Redox. Signal. 35 (2021) 1291–1307.
[15] G. Liu, X. Xie, Y. Li, et al., TrAC, Trends. Anal. Chem. 169 (2023) 117371.
[16] S. Zeng, X. Liu, Y.S. Kafuti, et al., Chem. Soc. Rev. 52 (2023) 5607–5651.
[17] Y. Chen, H. Jiang, T. Hao, et al., Chem. Biomed. Imaging 1 (2023) 590–619.
[18] L. Xiao, X. Sun, Z. Li, et al., Dyes Pigm. 216 (2023) 111385.
[19] J. Sun, X. Cao, W. Lu, et al., Theranostics 13 (2023) 1716.
[20] Y. Ji, S. Liu, J. Zhang, et al., Bioorg. Chem. 138 (2023) 106650.
[21] M. Ren, C. Zhou, L. Wang, et al., Chin. Chem. Lett. 34 (2023) 107646.
[22] Q. Ma, S. Xu, Z. Zhai, et al., Chem. Eur. J. 28 (2022) e202200828.
[23] L. He, H. Liu, J. Wu, et al., Chem. Asian J. 17 (2022) e202200388.
[24] X. Luo, Z. Cheng, R. Wang, et al., Anal. Chem. 93 (2021) 2490–2499.
[25] L. Shen, H. Liu, M. Jin, et al., Chin. Chem. Lett. 35 (2024) 109572.
[26] X. Wu, R. Wang, N. Kwon, et al., Chem. Soc. Rev. 51 (2022) 450–463.
[27] Y.L. Jung, S. Sarkar, J. Ha, et al., Bioconjugate. Chem. 33 (2022) 1543–1551.
[28] X. Wu, H. Li, E. Lee, J. Yoon, Chem 6 (2020) 2893–2901.
[29] J. Liu, X. Ma, C. Cui, et al., J. Med. Chem. 64 (2021) 17969–17978.
[30] H. Iwashita, E. Castillo, M.S. Messina, et al., Proc. Natl. Acad. Sci. U. S. A. 118 (2021) e2018513118.
[31] Z. Gao, A.J. Thompson, J.C. Paulson, et al., Angew. Chem. 130 (2018) 13726–13729.
[32] J. Jiang, Q. Tan, S. Zhao, et al., Chem. Commun. 55 (2019) 15000–15003.
[33] S. Wang, W. Tan, W. Lang, et al., Anal. Chem. 94 (2022) 7272–7277.
[34] Y. Li, C. Xue, Z. Fang, et al., Anal. Chem. 92 (2020) 15017–15024.
[35] Y. Li, H. Song, C. Xue, et al., Chem. Sci. 11 (2020) 5889–5894.
[36] G.L. Squadrito, R. Cueto, A.E. Splenser, et al., Arch. Biochem. Biophys. 376 (2000) 333–337.
[37] W. Qu, C. Niu, X. Zhang, et al., Talanta 197 (2019) 431–435.
[38] M.M. Tarpey, C.R. White, E. Suarez, et al., Circ. Res. 84 (1999) 1203–1211.
[39] B.K. Yoo, J.W. Choi, C.Y. Shin, et al., Neurochem. Int. 52 (2008) 1188–1197.
[40] X. Ren, Y. Ding, N. Lu, Eur. J. Pharmacol. 775 (2016) 50–56.
[41] C. Szabó, G. Ferrer-Sueta, B. Zingarelli, et al., J. Biol. Chem. 272 (1997) 9030–9036.
[42] H. Chen, C. Bai, X. Wang, Expert Rev. Respir. Med. 4 (2010) 773–783.